

## Supporting Information

### **Interfacial Modification via Aniline Molecules with Multiple Active Sites for Performance Enhancement of n-i-p Perovskite Solar Cells**

Zhiquan An<sup>a</sup>, Siying Chen<sup>a</sup>, Tao Lu<sup>a</sup>, Pengjun Zhao<sup>b</sup>, Xiaodong Yang<sup>a</sup>, Yang Li<sup>a,c,\*</sup>, Juan Hou<sup>a,\*</sup>

<sup>a</sup>Xinjiang Production & Construction Corps Key Laboratory of Advanced Energy Storage Materials and Technology, College of Science, Shihezi University, No. 221 Beisi Road, Shihezi, 832003, Xinjiang, China

<sup>b</sup>Xinjiang Technical Institute of Physics and Chemistry, Chinese Academy of Sciences, Urumqi 830011, Xinjiang, China

<sup>c</sup>Bingtuan Energy Development Institute, Shihezi University, No. 221 Beisi Road, Shihezi, 832003, Xinjiang, China

\* Corresponding Authors (J. Hou, Y. Li).

E-mail: [hjuan05@shzu.edu.cn](mailto:hjuan05@shzu.edu.cn) (J. Hou)

E-mail: [yang2022@shzu.edu.cn](mailto:yang2022@shzu.edu.cn) (Y. Li).

**First-principle calculations:**

In this work, Device Studio program provides a number of functions for performing visualization, modeling and simulation. And based on density functional theory (DFT), all our calculations are performed using DS-PAW software integrated in Device Studio program<sup>1, 2</sup>. The generalized gradient approximation (GGA) of the Perdew-Burke-Ernzerhof (PBE) functional is used as the exchange-correlation functional<sup>3</sup>. A vacuum thickness of 20 Å is built to avoid the interactions between adjacent layers. Slab models of three-layered  $\text{PbI}_2/\text{C}_9\text{H}_{10}\text{N}_2\text{O}_4$  and two-layered  $\text{PbI}_2/\text{C}_9\text{H}_{10}\text{N}_2\text{O}_4$  and their junction were constructed for simulation<sup>4</sup>. The Monkhorst-Pack k-point meshes of  $2 \times 1 \times 4$  is adopted for geometrical optimization and electronic structure calculations in unit cell of  $\text{PbI}_2/\text{C}_9\text{H}_{10}\text{N}_2\text{O}_4$ . The cutoff factor is set as 1. During optimization, all the structures were fully relaxed with the force and total energy convergence criteria of 0.883 eV Å and 1e-4eV, respectively. During adsorption and diffusion processes, the DFT-D2 method with Grimme correction is adopted to describe the long-range van der Waals interactions<sup>5, 6</sup>. Besides, three-layered of lead iodide and two-layered of lead iodide are used as substrates, and the k-points is set as  $2 \times 1 \times 4$ .

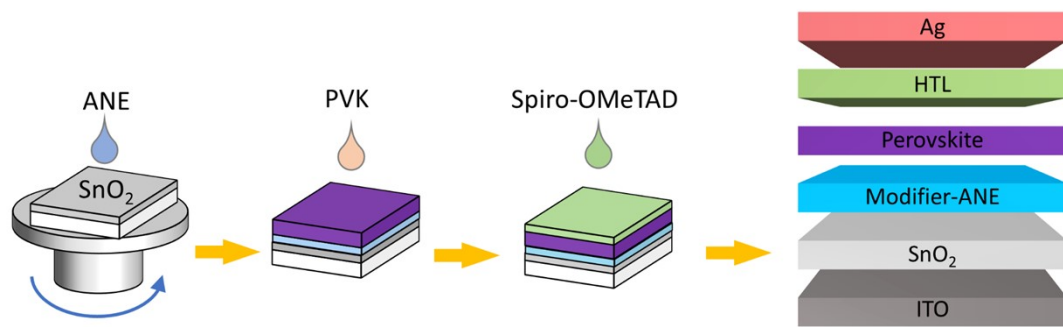


**Fig. S1.** The preparation process of the PSCs used in this work.

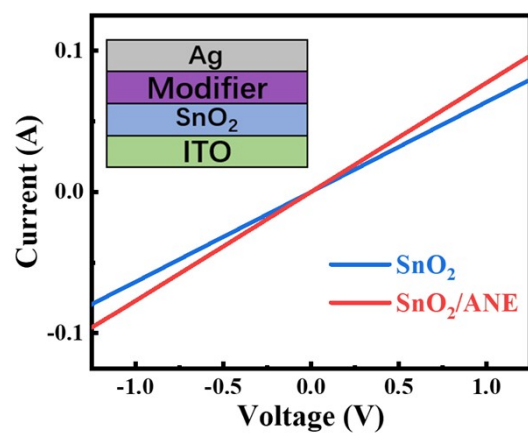


**Fig. S2.** I-V curves of the SnO<sub>2</sub> films without and with ANE.

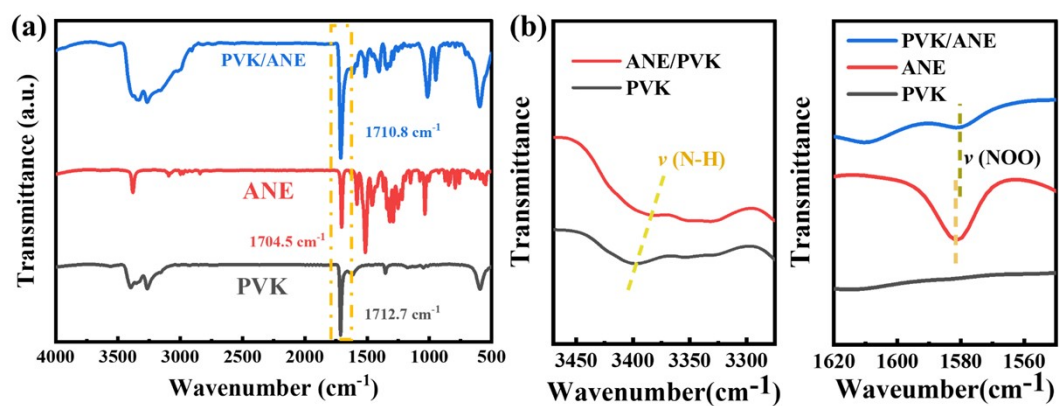


**Fig. S3.** FTIR spectra of PVK, ANE and PVK modified with ANE.

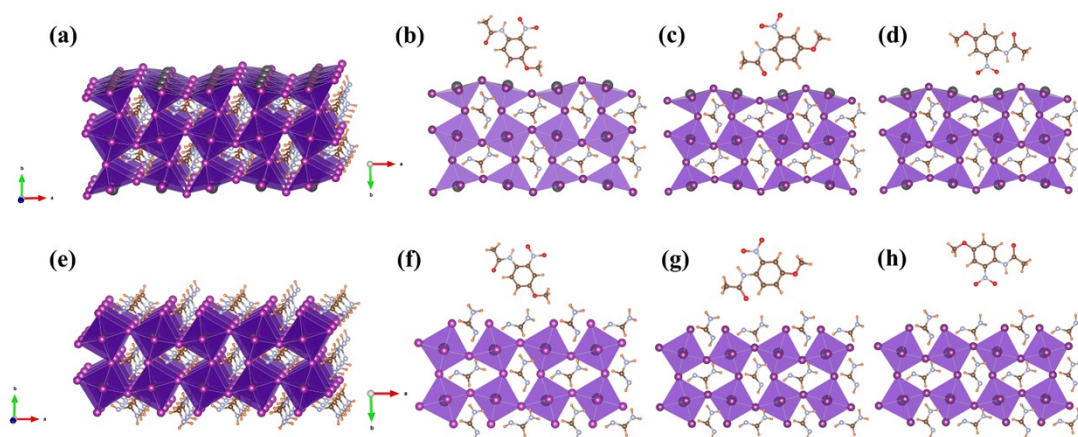


**Fig. S4.** Structure diagrams of unadsorbed substrate for (a)  $\text{PbI}_2$  and (e) FAI terminations. The interfaces for the inorganic  $\text{PbI}_2$  termination in contact with the different sites of ANE molecules (b-d), and the models were C-O-C, C=O and NOO sites, respectively. The interfaces for the organic FAI termination in contact with the different sites of ANE molecules (f-h), and the models were C-O-C, C=O and NOO sites, respectively.

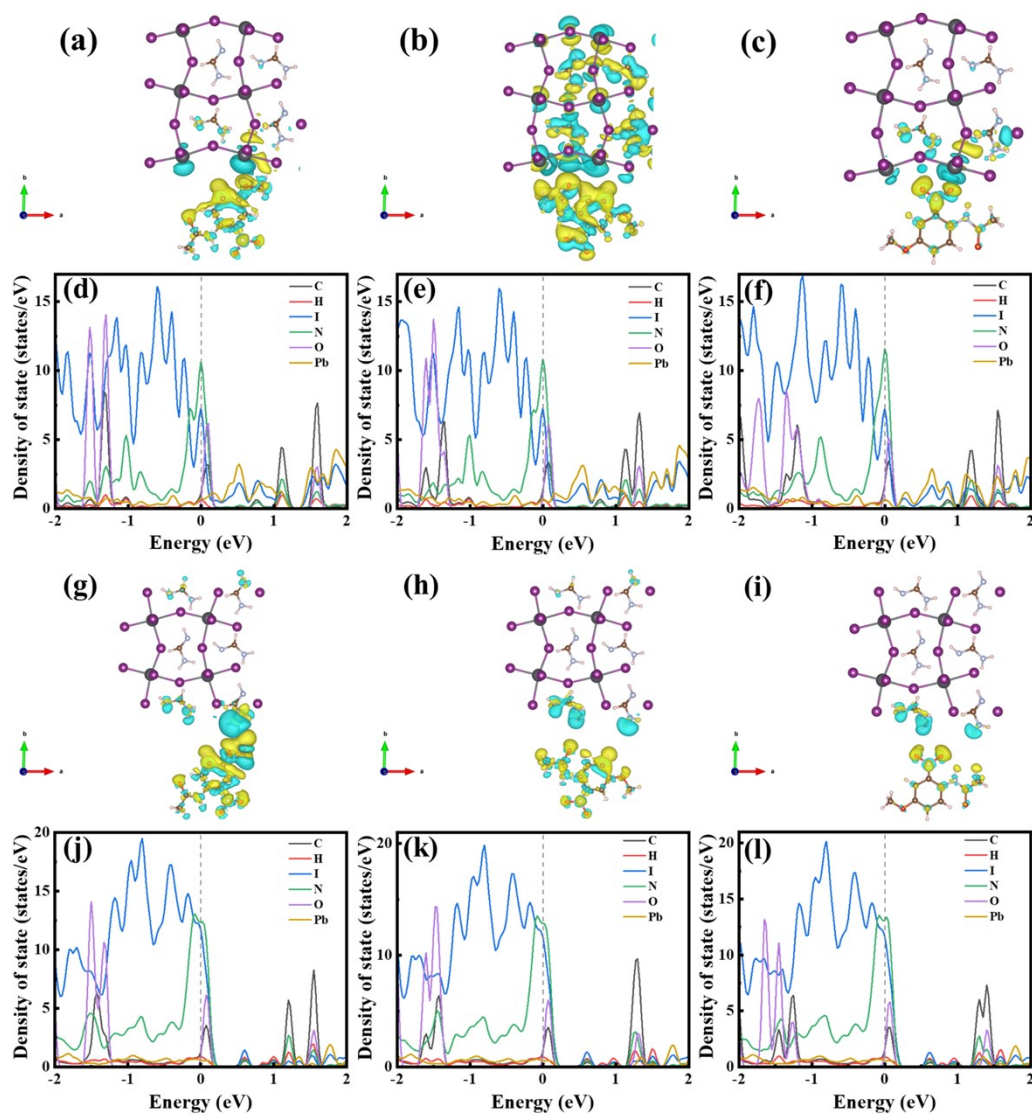


**Fig. S5.** Differential charge density and corresponding DOS diagram of contact between different active sites of ANE and PbI<sub>2</sub> and FAI terminations.

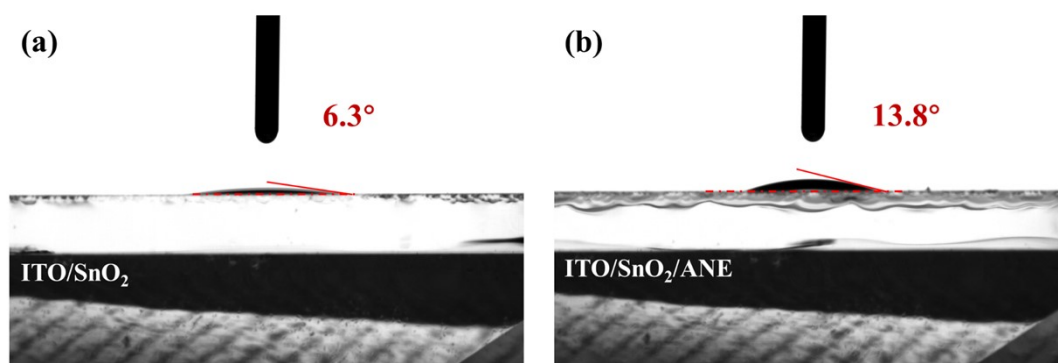


**Fig. S6.** Contact angle measurements of the (a) control and (b) modified SnO<sub>2</sub> films with ANE.



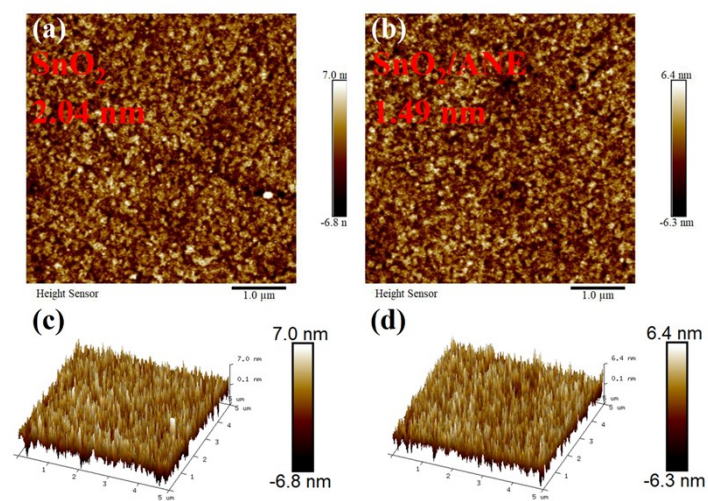


**Fig. S7.** AFM images of (a) the pristine  $\text{SnO}_2$  and (b)  $\text{SnO}_2/\text{ANE}$  films. 3D AFM images of (c)  $\text{SnO}_2$  and (d)  $\text{SnO}_2/\text{ANE}$  films.

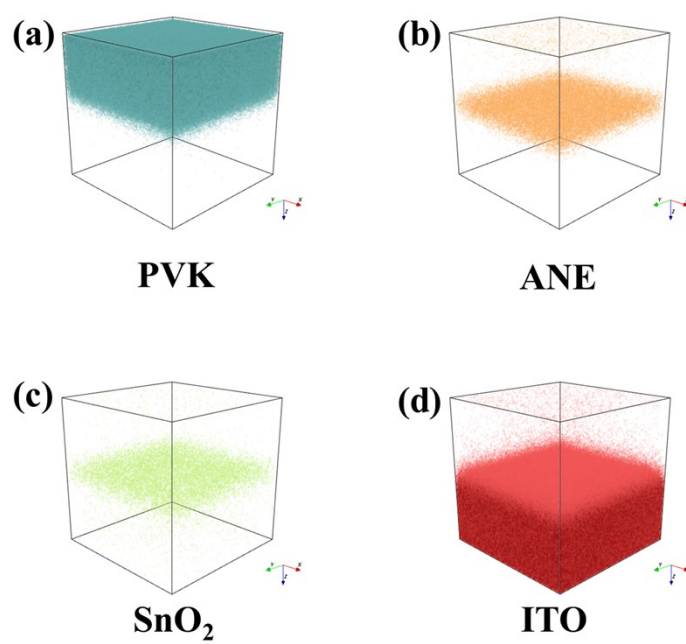


**Fig. S8.** ToF-SIMS 3D-depth profiles of the target devices with the structure of ITO/SnO<sub>2</sub>/ANE/perovskite.

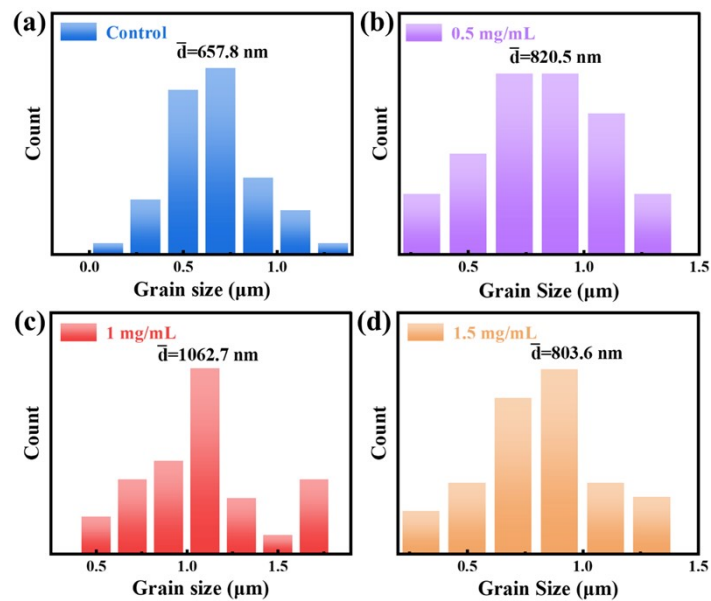


**Fig. S9.** Statistical distribution of PVK grains modified with different concentration of ANE.

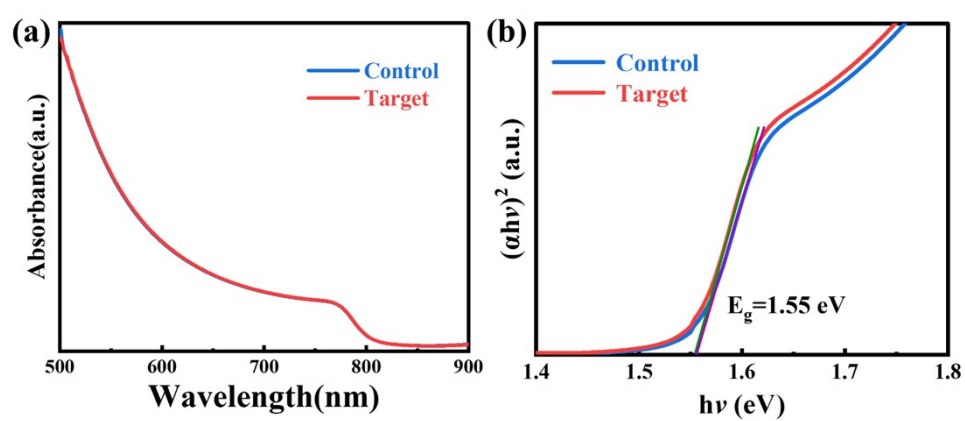


**Fig. S10.** (a) UV-Vis absorption spectra of the perovskite films without and with ANE passivation. The corresponding Tauc plot is shown in (b).

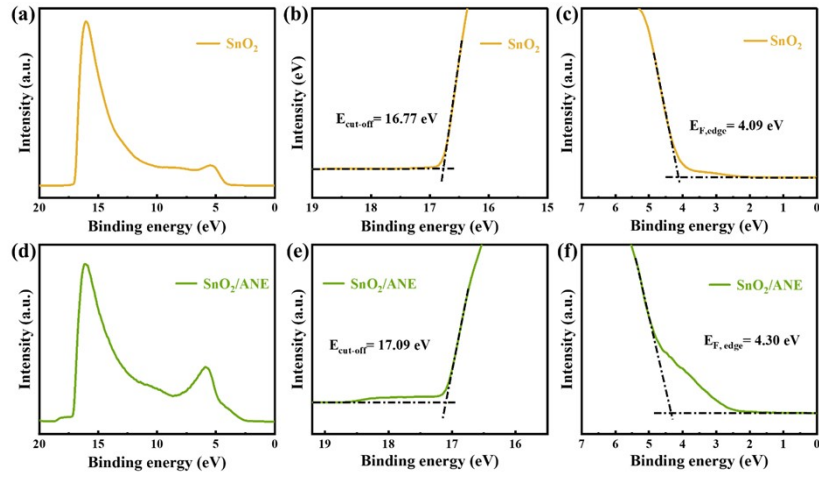


**Fig. S11.** (a) and (d) UPS full spectra. (b) and (e) UPS spectra describing the cut-off energy ( $E_{\text{cut-off}}$ ). (c) and (f) UPS spectra describing Fermi edge ( $E_{F,\text{edge}}$ ).

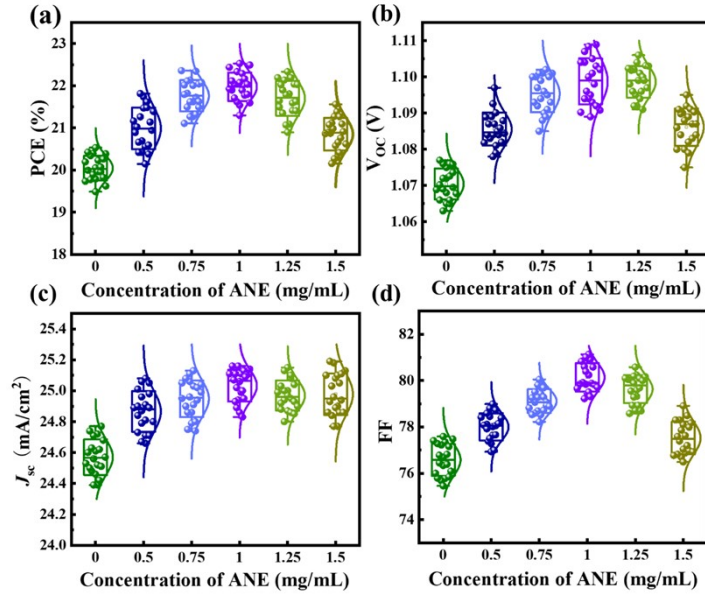


**Fig. S12.** Statistics of (a) PCE, (b) V<sub>OC</sub>, (c) J<sub>SC</sub>, and (d) FF of PSCs based on SnO<sub>2</sub> ETL modified by different concentrations of ANE.

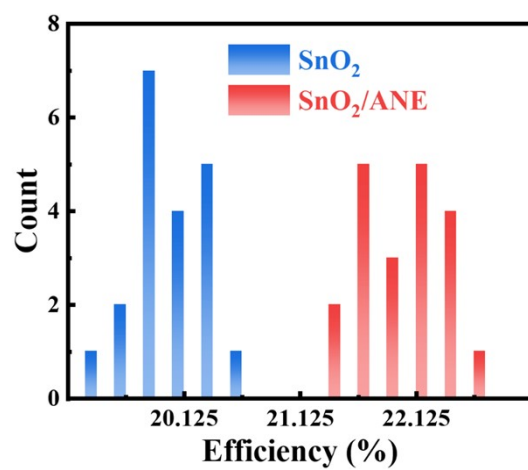


**Fig. S13.** Statistical distribution of PCEs of the PSCs based on the bare and modified  $\text{SnO}_2$  by ANE. The statistical data were obtained from 30 cells for each group.

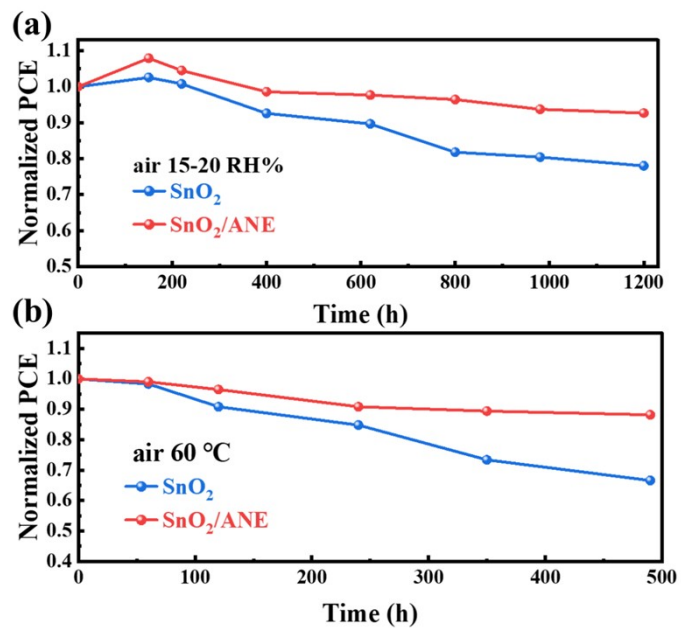


**Fig. S14.** (a) Moisture stability of the unsealed control and modified PSCs under an ambient condition with a relative humidity of 15–20% under dark. (b) Thermal stability of the unencapsulated control and modified devices at 60 °C in the air, under dark.



**Table S1.** Fitted results of TRPL curves of the perovskite films deposited on glass substrates with or without modifiers measured from perovskite side. The PVK represents the perovskite layer.

Samples	$\tau_1$ (ns)	$A_1$ (%)	$\tau_2$ (ns)	$A_2$ (%)	$\tau_{ave}$ (ns)
Glass/PVK	147.94	18.36	451.97	81.64	431.12
Glass/ANE/PVK	265.30	22.74	763.08	77.26	716.87

**Table S2.** Fitted results of TRPL curves of the perovskite films deposited on SnO<sub>2</sub> substrates with or without modifiers measured from perovskite side. The PVK represents the perovskite layer.

Samples	$\tau_1$ (ns)	$A_1$ (%)	$\tau_2$ (ns)	$A_2$ (%)	$\tau_{ave}$ (ns)
ITO/SnO <sub>2</sub> /PVK	144.69	6.03	507.67	93.97	501.15
ITO/SnO <sub>2</sub> /ANE/PVK	115.81	22.03	351.32	77.97	331.25

**Table S3.** The fitted EIS parameters of the devices based on SnO<sub>2</sub> and SnO<sub>2</sub>/ANE ETLs.

ETL	$R_s$ ( $\Omega$ )	$R_{ct}$ ( $\Omega$ )	$R_{rec}$ ( $\Omega$ )
SnO <sub>2</sub>	29.05	11806	49720
SnO <sub>2</sub> /ANE	43.01	7583	78330

**Table S4.** Photovoltaic parameters of the average performing control and target devices measured in RS and FS.

Device		$J_{SC}$ (mA/cm <sup>2</sup> )	$V_{OC}$ (V)	FF	PCE (%)	$R_s$ ( $\Omega$ )	$R_{sh}$ ( $\Omega$ )
Control	FS	24.52	1.068	0.7595	19.88	4.12	6173.58
	RS	24.53	1.072	0.7682	20.20	4.07	7052.25
Target	FS	25.12	1.106	0.8104	22.51	3.30	9034.97
	RS	25.14	1.108	0.8110	22.59	3.11	11084.62

## References

1. P. E. Blöchl, *Phys. Rev. B*, 1994, **50**, 17953-17979.
2. D. S. Hongzhiwei Technology, Version 2021A, China, 2021. Available online: <https://iresearch.net.cn/cloudSoftware>.
3. J. P. Perdew, K. Burke and M. Ernzerhof, *Phys. Rev. Lett.*, 1996, **77**, 3865-3868.
4. G. Kresse and D. Joubert, *Physical Review B*, 1999, **59**, 1758-1775.
5. S. Grimme, J. Antony, S. Ehrlich and H. Krieg, *J. Chem. Phys.*, 2010, **132**, 154104.
6. K. Parlinski, Z. Q. Li and Y. Kawazoe, *Phys. Rev. Lett.*, 1997, **78**, 4063-4066.